Dirac Polarons and Resistivity Anomaly in $ZrTe_5$ and $HfTe_5$

Bo Fu, Huan-Wen Wang, and Shun-Qing Shen*
Department of Physics, The University of Hong Kong, Pokfulam Road, Hong Kong, China

(Received 2 July 2020; revised 28 August 2020; accepted 20 November 2020; published 15 December 2020)

Resistivity anomaly, a sharp peak of resistivity at finite temperatures, in the transition-metal pentatellurides $ZrTe_5$ and $HfTe_5$ was observed four decades ago, and more exotic and anomalous behaviors of electric and thermoelectric transport were revealed in recent years. Here, we present a theory of Dirac polarons, composed by massive Dirac electrons and holes in an encircling cloud of lattice displacements or phonons at finite temperatures. The chemical potential of Dirac polarons sweeps the band gap of the topological band structure by increasing the temperature, leading to the resistivity anomaly. Formation of a nearly neutral state of Dirac polarons accounts for the anomalous behaviors of the electric and thermoelectric resistivity around the peak of resistivity.

DOI: 10.1103/PhysRevLett.125.256601

Introduction.—Resistivity in the transition-metal pentatellurides $ZrTe_5$ and $HfTe_5$ exhibits a sharp peak at a finite temperature T_p. The peak occurs approximately at a large range of temperatures from 50 to 200 K, but the exact value varies from sample to sample. The effect was observed forty years ago [1,2], but has yet to be understood very well. At the beginning, it was thought of as a structural phase transition, or occurrence of charge density wave. The idea was soon negated as no substantial evidence was found to support the picture [3–6]. The measurements of the Hall and Seebeck coefficients showed that the type of charge carriers dominating the electrical transport changes its sign around the peak, which indicates the chemical potential of the charge carriers sweeps the band gap around the transition temperature T_p [7–10]. Thus, the anomaly is believed to originate in the strong temperature dependence of the chemical potential and carrier mobility. In recent years, the advent of topological insulators revived extensive interest in exploring the physical properties of $ZrTe_5$ and $HfTe_5$. The first principles calculation suggested that the band structures of $ZrTe_5$ and $HfTe_5$ are topologically nontrivial in the layered plane or very close to the topological transition points [11]. Further studies uncover more exotic physics in these compounds [12–25], such as the chiral magnetic effect and three-dimensional quantum Hall effect. Other possible causes have been advanced much more recently [26–28], but the physical origin of the resistivity anomaly is still unclear. For example, it was suggested that a topological quantum phase transition might occur, and the gap closing and reopening give rise to the resistivity anomaly [28]. However, it contradicts the observation of the angle-resolved photoemission spectroscopy (ARPES) measurement [29,30].

Strong temperature dependence of the band structure [29] implies that the interaction between the Bloch electrons and the lattice vibrations, i.e., the electron-phonon interaction (EPI), is an indispensable ingredient for understanding the anomaly [31]. In this Letter, we consider an anisotropic Dirac model describing the low energy excitations of a weak topological insulator near the Fermi surface and EPI in $ZrTe_5$ and $HfTe_5$, and propose a theory of Dirac polarons for the resistivity anomaly at finite temperatures. The Dirac polarons are mixtures of massive Dirac electrons and holes encircling a cloud of phonons and are the effective charge carriers in the compounds. Increasing temperature will change the overlapping of the Dirac polarons drastically. The chemical potential of Dirac polarons sweeps the band gap from conduction bands to valence bands with increasing the temperature. Consequently, when the chemical potential of Dirac polarons locates around the middle of the band gap, the resistivity is enhanced drastically to form a pronounced peak at a finite temperature. The carriers dominating the charge transport change the sign around the transition. The formation of a nearly neutral state of Dirac polarons accounts for anomalous electric and magnetotransport properties in the compounds.

Finite temperature, spectral function, and quasiparticle properties.—The charge carriers in the conduction and valence bands of the bulk $ZrTe_5$ and $HfTe_5$ are strongly coupled together due to spin-orbit interaction and behave like massive Dirac fermions instead of conventional electrons in semiconductors and metals [13,32,33]. In the following, we only focus on $ZrTe_5$ for comparison with experimental measurement and theoretical calculation without loss of generality. When the electrons (or holes) are moving through the ionic lattices, the surrounding lattice will be displaced from the original equilibrium positions; consequently, the electrons (or holes) will be encircled by the lattice distortions, or phonons. At finite temperatures, Dirac polarons are composed of both massive Dirac electrons and holes in a cloud of phonons due to the

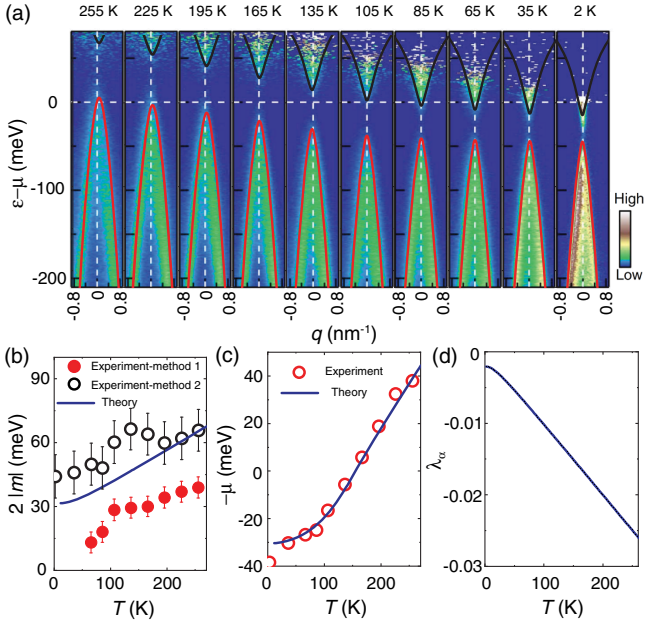

FIG. 1. (a) A comparison of the renormalized energy spectrums according to the theory (the solid lines) and the temperature-dependent band structures from ARPES measurement adopted from Fig. 2(b) in Ref. [29]. (b) The renormalized Dirac mass m due to the EPI, (c) the temperature dependent chemical potential μ, and (d) the velocity dressing function λ_α. The experiment data are extracted from Figs. 2(d) and 2(f) in Ref. [29]. The model parameters are set to be $v_x \simeq v_y = v_\perp = 4 \times 10^5$ m/s, $v_z = 0.5 \times 10^5$ m/s, $b_x \simeq b_y = b_\perp = 230$ meV nm^2, $d_x \simeq d_z = d_\perp = -225$ meV nm^2, $b_z = d_z = 0$ and $m = 12.0$ meV for all the figures if there is no further claiming. The carrier density used here is $n = 4 \times 10^{17}$ cm^{-3}.

thermal activation when the chemical potential is located around the band edges as illustrated in Fig. 1(a). The Hamiltonian describing the EPI in Dirac materials has the form [34], $\mathcal{H}_{\rm tot} = \mathcal{H}_{\rm Dirac} + \mathcal{H}_{\rm ph} + \mathcal{H}_{\rm ep}$. Here, the phonon part $\mathcal{H}_{\rm ph}$ is in the harmonic approximation, and the EPI part $\mathcal{H}_{\rm ep}$ is dominantly contributed by longitudinal acoustic phonons. The low-energy physics of the electronic states near the Fermi surface $\mathcal{H}_{\rm Dirac}$, can be well described by the anisotropic Dirac model [35],

$$\mathcal{H}_{\rm Dirac}(\mathbf{p}) = (d(\mathbf{p}) - \mu)I + \sum_{i=x,y,z} \hbar v_i p_i \alpha_i + m(\mathbf{p})\beta, \qquad (1)$$

where $\mathbf{p} = (p_x, p_y, p_z)$ is the relative momentum to the Γ point, v_i $(i = x, y, z)$ are the effective velocities in three directions. μ is the chemical potential. $d(\mathbf{p}) = \sum_{i=x,y,z} d_i p_i^2$ breaks the particle-hole symmetry and plays an essential role in the Dirac polaron physics. $m(\mathbf{p}) = m - \sum_{i=x,y,z} b_i p_i^2$ is the momentum dependent Dirac mass. The first principles calculation suggested that $ZrTe_5$ is possibly a weak topological insulator [11], and the ARPES measurement showed that there are no surface states within the band gap in its a–c plane (the layers stacking along the b axis) [11]. Thus, we consider an anisotropic case of $b_x \simeq b_y > 0$ and $b_z \leq 0$. The detailed analysis of the band topology can be found in Sec. SI of Ref. [36]. The Dirac matrices are chosen to be $\boldsymbol{\alpha} = \tau_x \otimes (\sigma_x, \sigma_y, \sigma_z)$ and $\beta = \tau_z \otimes \sigma_0$, where σ and τ are the Pauli matrices acting on spin and orbital space, respectively. The quantitative information about these physical properties, such as the Dirac velocity, the Dirac mass, or the energy gap can be extracted from the ARPES data [29,45,46]. To explore the EPI effect, we treat $\mathcal{H}_{\rm ep}$ as a perturbation to either electrons or phonons in the Migdal approximation [43] that the self-energy arises from the virtual exchange of a phonon at temperature T. Because of the spinor nature of Dirac electrons, the retarded self-energy can be recast in a matrix form as [36,47,48]

$$\Sigma^R_{\rm ep}(\mathbf{p}, \epsilon) = \Sigma_I(\mathbf{p}, \epsilon) + \lambda_\alpha(\mathbf{p}, \epsilon)\hbar v \mathbf{p} \cdot \boldsymbol{\alpha} + \Sigma_\beta(\mathbf{p}, \epsilon)\beta, \qquad (2)$$

where $\Sigma_I(\mathbf{p}, \epsilon)$ is the renormalization to the chemical potential μ, $\lambda_\alpha(\mathbf{p}, \epsilon)$ is the velocity dressing function, and $\Sigma_\beta(\mathbf{p}, \epsilon)$ is the renormalization to the Dirac mass m.

The quasiparticle properties of the Dirac polaron can be obtained by the poles of the retarded Green's function $G^R(\mathbf{p}, \epsilon) = [\epsilon - \mathcal{H}_{\rm Dirac}(\mathbf{p}) - \Sigma^R(\mathbf{p}, \epsilon)]^{-1}$, which, in the complex plane, its real part gives the spectrum of the quasiparticle, and the imaginary part gives its lifetime. The self-energy $\Sigma^R(\mathbf{p}, \epsilon) = \Sigma^R_{\rm ep}(\mathbf{p}, \epsilon) + \Sigma^R_{\rm imp}(\mathbf{p}, \epsilon)$ includes the contribution from the impurities scattering. The spectral function of the quasiparticle properties of Dirac polarons is given by the imaginary part of $G^R(\mathbf{p}, \epsilon)$,

$$A_\zeta(\mathbf{p}, \epsilon) = -\frac{1}{\pi} \langle \zeta s \mathbf{p} | \mathrm{Im} G^R(\mathbf{p}, \epsilon) | \zeta s \mathbf{p} \rangle, \qquad (3)$$

where $|\zeta s \mathbf{p}\rangle$ are the band states with the band indices $\zeta = \pm$ for the conduction and valence band, and for the spin indices $s = \pm$. In the absence of disorder and EPI, $A_\zeta(\mathbf{p}, \epsilon)$ is a δ function reflecting that $\mathbf{p}$ is a good quantum number, and all its weight ratio is precisely at $\epsilon = \xi^\zeta_{\mathbf{p}}$. In the presence of disorder and EPI, at low temperatures, $A_\zeta(\mathbf{p}, \epsilon)$ exhibits a sharp peak of the Lorentzian type due to a long lifetime. As temperature increases, $A_\zeta(\mathbf{p}, \epsilon)$ maintains the Lorentzian line shape but becomes broader due to the increasing of the scattering rate, and the peak position moves to the positive energy due to the renormalization of the energy level. The trajectories of the peaks of the spectral function give us the renormalized dispersion $\tilde{\xi}_\zeta(\mathbf{p})$. As shown in Fig. 1(a), we plot the derived energy dispersions $\tilde{\xi}_\zeta(\mathbf{p})$ for different temperatures with the black and red lines corresponding to the conduction and valence bands, respectively. The ARPES data extracted from Ref. [29] are also presented as the background for a comparison. The excellent agreement can be found between our theoretical calculations and the experiment data. The overall band structure shifts up to higher energy with increasing temperature. The peak structure of the spectral function can be

clearly observed in the temperature range considered, which suggests that a quasiparticle picture is still appropriate at low energy, and the EPI largely preserves the weakly perturbed Fermi-liquid behavior.

The renormalized Dirac mass m is given by the difference between two energy levels $\tilde{\xi}_+(\mathbf{0})$ and $\tilde{\xi}_-(\mathbf{0})$ for the states at the band edge $(\mathbf{p}=0)$: $\bar{m}=\frac{1}{2}[\tilde{\xi}_+(\mathbf{0})-\tilde{\xi}_-(\mathbf{0})]$. At higher temperature, the effective mass varies with T as $\bar{m}\simeq m+g_mT$ shown in Fig. 1(b). The coefficient g_m are determined by the band structure and the EPI strength (see the details in Ref. [36]). For Dirac materials, the renormalization of the energy levels is attributed to xthe contributions from both intraband and interband scatterings. With increasing temperature, the more phonon modes with high momenta are active, the larger the renormalization is. The chemical potential is determined by the charge carriers density $n=\int_{|\bar{m}|}^{\infty}d\omega[\bar{\nu}_+(\omega)n_F(\omega-\mu)-\bar{\nu}_-(-\omega)n_F(\omega+\mu)]$ where $n_F(x)=[\exp(x/k_BT)+1]^{-1}$ is the Fermi distribution function and $\bar{\nu}_\pm(\omega)$ are the renormalized density of states for the conduction and valence bands, respectively. In the band structure of $ZrTe_5$, the particle-hole symmetry is broken and the valence band is narrower than the conduction band. At the fixed n, the temperature dependence $\mu(T)$ is plotted in Fig. 1(c). The calculated results demonstrate that the chemical potential sweeps over the energy band gap of the massive Dirac particles with increasing temperature. At low temperatures, $\mu(T)\approx\mu(0)-(\pi^2/6)(k_BT)^2(d\bar{\nu}_\pm(\omega)/d\omega/\bar{\nu}_\pm(\omega))|_{\omega=\mu(0)}$ shows a quadratic temperature dependence by means of the Sommerfeld expansion. $\mu(T)=0$ means the chemical potential is located at the midgap, which approximately defines the transition temperature T_p around. At high temperatures, due to the strong particle-hole asymmetry and the relatively low carrier density, the chemical potential shifts into the valence band in a relatively linear fashion with increasing temperature. The velocity dressing function λ_α as a function of T is plotted in Fig. 1(d). The velocity for Dirac polaron decreases linearly with T for higher temperature and saturates a constant value for lower temperature.

The resistivity anomaly.—With the phonon-induced self-energy in hand, we are ready to present the electrical resistivity as a function of temperature by means of the linear response theory [34,36]. At finite temperatures, the conductivities and thermoelectric coefficients are contributed from both the electronlike and holelike bands after the phonon-induced renormalization. The two contributions are weighted by the negative energy derivative of the Fermi-Dirac function, whose value is nearly zero except for energies within a narrow window of k_BT near the chemical potential μ. Figure 2(a) reproduces the resistivity peak at several initial chemical potentials μ or, equivalently, carrier densities at $T=0$. For the initial $\mu(T=0)$ (>0) locating in the conduction band, as it moves down to the valance band with increasing temperature, it will inevitably sweep over the band gap. When $T=T_p$, the effective

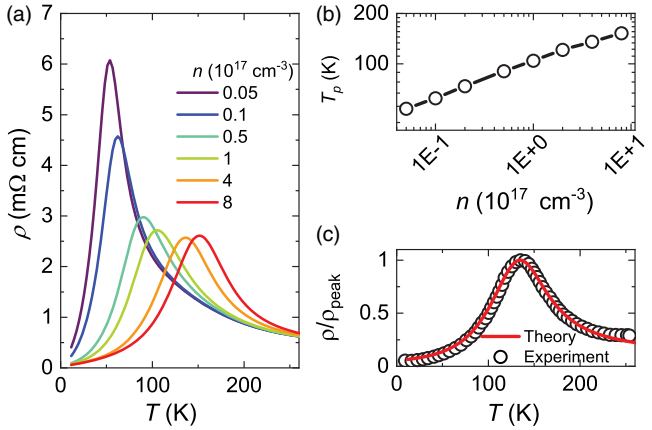

FIG. 2. (a) The zero-field resistivity ρ as a function of temperature for several carrier densities n. (b) The peak temperature T_p as a function of the carrier density. (c) The comparison of the experimental data and theoretical prediction by using the same parameters as Fig. 1. The experimental data are extracted from Fig. 1(d) in Ref. [29]. Both resistivity curves have been normalized to their maximum values ρ_{peak}.

chemical potential lies around the middle of the effective band gap $\mu(T=T_p)\simeq 0$ and the resistivity reaches the maximum. As the n-type carrier concentration is decreased, the resistivity peak will move to the lower temperature with the higher magnitude. The peak temperature as a function of the carrier density is plotted in Fig. 2(b). For a lower carrier concentration, the chemical potential reaches the middle of the band gap with a lower temperature. The height of the resistivity peak is determined by the ratio $\bar{m}(T_p)/(k_BT_p)$. By increasing the ratio, the peak height increases drastically, and becomes divergent if $\bar{m}(T_p)\gg k_BT_p$. It explains why, in some experiments with extreme low carrier concentration, no resistivity peak is observed [20,49], which can be regarded as the situation of $T_p\sim 0$. Thus, the sweeping chemical potential over the band gap of Dirac fermions gives rise to the resistivity anomaly at finite temperatures. We use the model parameters in Fig. 1 to calculate the resistivity, which is in good agreement with the experimental data as shown in Fig. 2(c). The slight deviation at the high temperature might be caused by neglecting the contributions from the optical modes of phonons.

Sign change of the Hall and Seebeck coefficients.—The resistivity anomaly is always accompanied by the sign change of the Hall and Seebeck coefficients around the transition temperature [8,23,40,50–52], which can be reproduced in the present theory. As shown in Fig. 3(a), for a positive $\mu(T=0)$ or n-type carriers, by increasing the temperature, the Hall coefficient $(R_H=\partial\rho_{xy}/\partial B|_{B=0})$ first maintains its value $(1/en)$ at low temperature, decreases down until reaching the minimum. Then R_H changes from the negative to a positive sign at some temperature and continues to decrease down to nearly zero

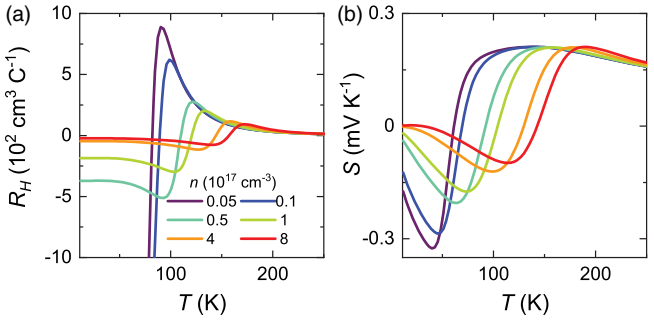

FIG. 3. (a) The Hall coefficient R_H and (b) the Seebeck coefficient S as functions of temperature of several carrier densities n.

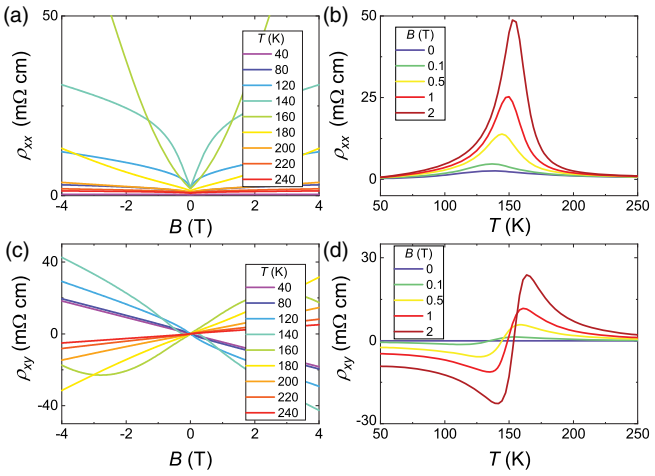

FIG. 4. The magnetic field dependence of (a) the transverse magnetoresistance ρ_{xx} and (c) the Hall resistivity ρ_{xy} for different temperatures. The temperature dependence of (b) ρ_{xx} and (d) ρ_{xy} for different magnetic fields.

at high temperatures. The sign change of R_H indicates that the electron-dominated transport is transformed into the hole-dominated as the chemical potential moves from the conduction band to the valence band. As the carrier concentration decreases, the Hall coefficient crosses 0 at a lower temperature with a larger maximum. In Fig. 3(b), the Seebeck coefficient S_{xx} also reveals a systematic shift in temperature as the carrier density increases. For each curve with fixed carrier density, S_{xx} displays similar nonmonotonic temperature dependence as R_H, except that S_{xx} starts from absolute zero and exhibits a relatively large positive (p-type) Seebeck coefficient at high temperatures. At low temperatures, the chemical potential lies deep in the bulk band, the Mott formula relates the thermoelectric conductivity with the derivative of the electrical conductivity for the thermopower $S_{xx} = (\pi^2 k_B^2 T/3e)(d\sigma(\omega)/d\omega/\sigma(\omega))|_{\omega=\mu}$ [53] with $\sigma(\omega)$ as the energy-dependent conductivity. The conductivity $\sigma(\omega)$ is proportional to the square of the group velocity. Hence, as chemical potential locates in the conduction band, S_{xx} is negative (n-type) and decreases with increasing temperature. S_{xx} attains its largest value when n is tiny but nonvanishing and varies rapidly with the temperature around T_p. [54]. T_p decreases with the reduction of the n-type carrier concentration and, at zero temperature, qualitatively agrees with previous measurements for single crystals with different carrier concentrations [52]. Near $T = T_p$ and if the band gap $\bar{m}(T_p)$ is comparably smaller than the thermal energy $k_B T_p$, either R_H or S_{xx} is linear in temperature and the system enters a nearly neutral state of Dirac polarons due to the strong thermal activation.

Magnetotransport in nearly neutral state of Dirac polarons.—The presence of an external magnetic field reveals the exotic behaviors of magnetoresistivity near the transition temperature [10,15,23,26,51,55]. Without loss of generality, we assume the magnetic field B is along the z direction. As shown in Fig. 4(a), the transverse magnetoresistivity $\rho_{xx}(B)$ displays significantly different behaviors for temperature above and below T_p. Below 120 K, a narrow dip is observed around zero magnetic field and above 200 K, ρ_{xx} shows a quadratic field dependence. Approaching the peak temperature, ρ_{xx} becomes large and nonsaturating. We plot the resistivity as a function of temperature for different magnetic fields. As shown in Fig. 4(b), $\rho_{xx}(B)$ displays striking resistivity peaks when the temperature crosses the region of the neutral state of Dirac polarons. The peak is strongly enhanced with increasing magnetic field, and even becomes nonsaturated. Its position is observed to shift slightly to a higher temperature with the field increasing, i.e., T_p is a function of B. This effect has been reported experimentally in Refs. [15,23]. The appearance of giant and nonsaturated transverse magnetoresistivity can be viewed as the electrical signature of the neutral state of Dirac polarons. As shown in Fig. 4(c), the slope of the Hall resistivity ρ_{xy} is negative, indicating an electron-dominated charge transport. As the temperature increases, the nonlinearity of ρ_{xy} becomes more apparent. In the intermediate temperature ($120 \sim 180$ K) around T_p, due to the formation of the nearly neutral state of Dirac polarons, the slope of the Hall resistivity changes from positive (hole type) at low magnetic field to negative (electron type) at high field, showing a zigzag shaped profile. At high temperature (above 200 K), the hole carrier dominates the charge transport, thus, the slope of ρ_{xy} become positive. The effect of an applied magnetic field on ρ_{xy} as a function of temperature is shown in Fig. 4(d). There is a systematic shift to the higher temperatures with increasing field. The calculated ρ_{xx} and ρ_{xy} as functions of either T or B are in excellent agreement with the experimental measurements in $ZrTe_5$ and $HfTe_5$ [23,26,51,55]. Last, we want to point out the differences between the present theory and the two-carrier model for magnetoresistance [56]. The two-carrier model commonly requires that the Fermi surface is composed of both electron and hole pockets and predicts a quadratical

magnetoresistance, while the present theory only involves a single Dirac band crossing the Fermi surface and the multicarrier transport is attributed to thermal excitation over a wide range of temperatures.

Discussion.—From an experimental standpoint, a temperature-dependent effective carrier density can be deduced from the Hall measurement. The shift of the chemical potential or effective carrier density with the variation of temperature is the key issue to the resistivity anomaly. With no absorption or desorption process through extrinsic doping, the temperature dependent variation of effective density of charge carriers seems to violate the conservation law of the total charge. However, the relative contribution from each band of carriers to the total Hall effect also depends on its ability to respond to the applied magnetic field such as velocity and mobility. In Dirac materials with extreme low carrier density and tiny band gap, the strong particle-hole asymmetry will induce a significant temperature variation of the chemical potential, even shifts from conduction band to valence band. Consequently, the effective carrier density also displays strong temperature dependence.

We thank Li-Yuan Zhang, Nan-Lin Wang, and Chen-Jie Wang for helpful discussions. This work was supported by the Research Grants Council, University Grants Committee, Hong Kong under Grants No. 17301220 and No. C7036-17W, and the National Key R&D Program of China under Grant No. 2019YFA0308603.

*sshen@hku.hk

[1] S. Okada, T. Sambongi, and M. Ido, Giant resistivity anomaly in $ZrTe_5$, J. Phys. Soc. Jpn. **49**, 839 (1980).

[2] M. Izumi, K. Uchinokura, and E. Matsuura, Anomalous electrical resistivity in HfTe5, Solid State Commun. **37**, 641 (1981).

[3] F. DiSalvo, R. Fleming, and J. Waszczak, Possible phase transition in the quasi-one-dimensional materials $ZrTe_5$ or $HfTe_5$, Phys. Rev. B **24**, 2935 (1981).

[4] S. Okada, T. Sambongi, M. Ido, Y. Tazuke, R. Aoki, and O. Fujita, Negative evidences for charge/spin density wave in $ZrTe_5$, J. Phys. Soc. Jpn. **51**, 460 (1982).

[5] D. Bullett, Absence of a phase transition in $ZrTe_5$, Solid State Commun. **42**, 691 (1982).

[6] H. Fjellvag and A. Kjekshus, Structural properties of $ZrTe_5$ and $HfTe_5$ as seen by powder diffraction, Solid State Commun. **60**, 91 (1986).

[7] M. Izumi, K. Uchinokura, E. Matsuura, and S. Harada, Hall effect and transverse magnetoresistance in a low-dimensional, Solid State Commun. **42**, 773 (1982).

[8] T. Jones, W. Fuller, T. Wieting, and F. Levy, Thermoelectric power of $HfTe_5$ and $ZrTe_5$, Solid State Commun. **42**, 793 (1982).

[9] R. T. Littleton Iv, T. M. Tritt, J. W. Kolis, and D. Ketchum, Transition-metal pentatellurides as potential low-temperature thermoelectric refrigeration materials, Phys. Rev. B **60**, 13453 (1999).

[10] T. M. Tritt, N. D. Lowhorn, R. T. Littleton Iv, A. Pope, C. R. Feger, and J. W. Kolis, Large enhancement of the resistive anomaly in the pentatelluride materials $HfTe_5$ and $ZrTe_5$ with applied magnetic field, Phys. Rev. B **60**, 7816 (1999).

[11] H. Weng, X. Dai, and Z. Fang, Transition-Metal Pentatelluride $ZrTe_5$ and $HfTe_5$: A Paradigm for Large-Gap Quantum Spin Hall Insulators, Phys. Rev. X **4**, 011002 (2014).

[12] Z.-G. Chen, R. Chen, R. Zhong, J. Schneeloch, C. Zhang, Y. Huang, F. Qu, R. Yu, Q. Li, G. Gu, and N. Wang, Spectroscopic evidence for bulk-band inversion and three-dimensional massive Dirac fermions in $ZrTe_5$, Proc. Natl. Acad. Sci. U.S.A. **114**, 816 (2017).

[13] G. Manzoni, L. Gragnaniello, G. Autès, T. Kuhn, A. Sterzi, F. Cilento, M. Zacchigna, V. Enenkel, I. Vobornik, L. Barba, F. Bisti, Ph. Bugnon, A. Magrez, V. N. Strocov, H. Berger, O. V. Yazyev, M. Fonin, F. Parmigiani, and A. Crepaldi, Evidence for a Strong Topological Insulator Phase in $ZrTe_5$, Phys. Rev. Lett. **117**, 237601 (2016).

[14] Y. Jiang, J. Wang, T. Zhao, Z. L. Dun, Q. Huang, X. S. Wu, M. Mourigal, H. D. Zhou, W. Pan, M. Ozerov, D. Smirnov, and Z. Jiang, Unraveling the Topological Phase of $ZrTe_5$ via Magnetoinfrared Spectroscopy, Phys. Rev. Lett. **125**, 046403 (2020).

[15] Q. Li, D. E. Kharzeev, C. Zhang, Y. Huang, I. Pletikosic, A. Fedorov, R. Zhong, J. Schneeloch, G. Gu, and T. Valla, Chiral magnetic effect in $ZrTe_5$, Nat. Phys. **12**, 550 (2016).

[16] Y. Zhou, J. Wu, W. Ning, N. Li, Y. Du, X. Chen, R. Zhang, Z. Chi, X. Wang, X. Zhu, P.o Lu, C. Ji, X. Wan, Z. Yang, J. Sun, W. Yang, M. Tian, Y. Zhang, and H.-k. Mao, Pressure-induced superconductivity in a three-dimensional topological material $ZrTe_5$, Proc. Natl. Acad. Sci. U.S.A. **113**, 2904 (2016).

[17] P. Li, C. H. Zhang, J. W. Zhang, Y. Wen, and X. X. Zhang, Giant planar Hall effect in the Dirac semimetal $ZrTe_{5-\delta}$, Phys. Rev. B **98**, 121108(R) (2018).

[18] H. Wang, H. Liu, Y. Li, Y. Liu, J. Wang, J. Liu, J.-Y. Dai, Y. Wang, L. Li, J. Yan, D. Mandrus, X. C. Xie, and J. Wang, Discovery of log-periodic oscillations in ultraquantum topological materials, Sci. Adv. **4**, eaau5096 (2018).

[19] H. Wang, Y. Liu, Y. Liu, C. Xi, J. Wang, J. Liu, Y. Wang, L. Li, S. P. Lau, M. Tian, J. Yan, D. Mandrus, J. Y. Dai, H. Liu, X. C. Xie, and J. Wang, Log-periodic quantum magneto-oscillations and discrete-scale invariance in topological material HfTe5, Natl. Sci. Rev. **6**, 914 (2019).

[20] T. Liang, J. Lin, Q. Gibson, S. Kushwaha, M. Liu, W. Wang, H. Xiong, J. A. Sobota, M. Hashimoto, P. S. Kirchmann, Z. Shen, R. J. Cava, and N. P. Ong, Anomalous Hall effect in $ZrTe_5$, Nat. Phys. **14**, 451 (2018).

[21] J. L. Zhang, C. M. Wang, C. Y. Guo, X. D. Zhu, Y. Zhang, J. Y. Yang, Y. Q. Wang, Z. Qu, L. Pi, H.-Z. Lu, and M. L. Tian, Anomalous Thermoelectric Effects of $ZrTe_5$ in and beyond the Quantum Limit, Phys. Rev. Lett. **123**, 196602 (2019).

[22] J. Hu, M. Caputo, E. B. Guedes, S. Tu, E. Martino, A. Magrez, H. Berger, J. H. Dil, H. Yu, and J.-P. Ansermet, Large magnetothermopower and anomalous Nernst effect in $ZrTe_5$, Phys. Rev. B **100**, 115201 (2019).

[23] F. Tang, Y. Ren, P. Wang, R. Zhong, J. Schneeloch, S. A. Yang, K. Yang, P. A. Lee, G. Gu, Z. Qiao, and L. Zhang, Three-dimensional quantum Hall effect and metal-insulator transition in $ZrTe_5$, Nature (London) **569**, 537 (2019).

[24] P. Wang, Y. Ren, F. Tang, P. Wang, T. Hou, H. Zeng, L. Zhang, and Z. Qiao, Approaching three-dimensional quantum Hall effect in bulk $HfTe_5$, Phys. Rev. B **101**, 161201(R) (2020).

[25] R. Y. Chen, S. J. Zhang, J. A. Schneeloch, C. Zhang, Q. Li, G. D. Gu, and N. L. Wang, Optical spectroscopy study of the three-dimensional Dirac semimetal $ZrTe_5$, Phys. Rev. B **92**, 075107 (2015).

[26] L.-X. Zhao, X.-C. Huang, Y.-J. Long, D. Chen, H. Liang, Z.-H. Yang, M.-Q. Xue, Z.-A. Ren, H.-M. Weng, Z. Fang, X. Dai, and G.-F. Chen, Anomalous magneto-transport behavior in transition metal pentatelluride $HfTe_5$, Chin. Phys. Lett. **34**, 037102 (2017).

[27] P. Shahi, D. J. Singh, J. P. Sun, L. X. Zhao, G. F. Chen, Y. Y. Lv, J. Li, J.-Q. Yan, D. G. Mandrus, and J.-G. Cheng, Bipolar Conduction as the Possible Origin of the Electronic Transition in Pentatellurides: Metallic vs Semiconducting Behavior, Phys. Rev. X **8**, 021055 (2018).

[28] B. Xu, L. Zhao, P. Marsik, E. Sheveleva, F. Lyzwa, Y. Dai, G. Chen, X. Qiu, and C. Bernhard, Temperature-Driven Topological Phase Transition and Intermediate Dirac Semimetal Phase in $ZrTe_5$, Phys. Rev. Lett. **121**, 187401 (2018).

[29] Y. Zhang *et al.*, Electronic evidence of temperature-induced Lifshitz transition and topological nature in $ZrTe_5$, Nat. Commun. **8**, 15512 (2017).

[30] Y. Zhang *et al.*, Temperature-induced Lifshitz transition in topological insulator candidate $HfTe_5$, Sci. Bull. **62**, 950 (2017).

[31] M. Rubinstein, $HfTe_5$ and $ZrTe_5$: Possible polaronic conductors, Phys. Rev. B **60**, 1627 (1999).

[32] R. Wu, J.-Z. Ma, S.-M. Nie, L.-X. Zhao, X. Huang, J.-X. Yin, B.-B. Fu, P. Richard, G.-F. Chen, Z. Fang, X. Dai, H.-M. Weng, T. Qian, H. Ding, and S. H. Pan, Evidence for Topological Edge States in a Large Energy Gap Near the Step Edges on the Surface of $ZrTe_5$, Phys. Rev. X **6**, 021017 (2016).

[33] X.-B. Li, W.-K. Huang, Y.-Y. Lv, K.-W. Zhang, C.-L. Yang, B.-B. Zhang, Y. B. Chen, S.-H. Yao, J. Zhou, M.-H. Lu, L. Sheng, S.-C. Li, J.-F. Jia, Q.-K. Xue, Y.-F. Chen, and D.-Y. Xing, Experimental Observation of Topological Edge States at the Surface Step Edge of the Topological Insulator $ZrTe_5$, Phys. Rev. Lett. **116**, 176803 (2016).

[34] G. D. Mahan, *Many-Body Physics*, 2nd ed. (Plenum Press, New York, 1990).

[35] S. Q. Shen, *Topological Insulators*, 2nd ed., Springer Series in Solid-State Sciences Vol. 187 (Springer, Singapore, 2017).

[36] See Supplemental Material at http://link.aps.org/supplemental/10.1103/PhysRevLett.125.256601 for details of (Sec. SI) the model Hamiltonian for Anisotropic Dirac materials (Sec. SII) the model for electron-phonon interaction, (Sec. SIII) the phonon-induced self-energy, (Sec. SIV) the renormalization of the energy level of the Dirac polaron, (Sec. SV) the vertex correction beyond Migdal's approximation, (Sec. SVI) the vertex corrections to the electron-phonon self-energy from the disorder effect, and (Sec. SVII) finite temperature conductivity, which includes Refs. [30,34,37–44].

[37] L. Fu and C. L. Kane, Topological insulators with inversion symmetry, Phys. Rev. B **76**, 045302 (2007).

[38] J. Zhu, T. Feng, S. Mills, P. Wang, X. Wu, L. Zhang, S. T. Pantelides, X. Du, and X. Wang, Record-low and anisotropic thermal conductivity of a quasi-one-dimensional bulk ZrTe5 single crystal, ACS Appl. Mater. Interfaces **10**, 40740 (2018).

[39] N. Aryal, X. Jin, Q. Li, A. M. Tsvelik, and W. Yin, Topological phase transition and phonon-space Dirac topology surfaces in ZrTe5, arXiv:2004.13326.

[40] W. Zhang, P. Wang, B. Skinner, R. Bi, V. Kozii, C.-W. Cho, R. Zhong, J. Schneeloch, D. Yu, G. Gu, L. Fu, X. Wu, and L. Zhang, Observation of a thermoelectric Hall plateau in the extreme quantum limit, Nat. Commun. **11**, 1046 (2020).

[41] P. Streda, Quantised Hall effect in a two-dimensional periodic potential, J. Phys. C **15**, L1299 (1982).

[42] H. W. Wang, B. Fu, and S. Q. Shen, Intrinsic magnetoresistance in three-dimensional Dirac materials with low carrier densityPhys. Rev. B **98**, 081202(R) (2018).

[43] A. B. Migdal, Interaction between electrons and lattice vibrations in a normal metal, Sov. Phys. JETP **34**, 996 (1958).

[44] E. Akkermans and G. Montambaux, *Mesoscopic Physics of Electrons and Photons* (Cambridge University Press, Cambridge, England, 2007).

[45] L. Moreschini, J. C. Johannsen, H. Berger, J. Denlinger, C. Jozwiack, E. Rotenberg, K. S. Kim, A. Bostwick, and M. Grioni, Nature and topology of the low-energy states in $ZrTe_5$, Phys. Rev. B **94**, 081101(R) (2016).

[46] G. Manzoni, A. Sterzi, A. Crepaldi, M. Diego, F. Cilento, M. Zacchigna, Ph. Bugnon, H. Berger, A. Magrez, M. Grioni, and F. Parmigiani, Ultrafast Optical Control of the Electronic Properties of $ZrTe_5$, Phys. Rev. Lett. **115**, 207402 (2015).

[47] I. Garate, Phonon-Induced Topological Transitions, and Crossovers in Dirac Materials, Phys. Rev. Lett. **110**, 046402 (2013).

[48] K. Saha and I. Garate, Phonon-induced topological insulation, Phys. Rev. B **89**, 205103 (2014).

[49] J. Mutch, W.-C. Chen, P. Went, T. Qian, I. Z. Wilson, A. Andreev, C.-C. Chen, and J.-H. Chu, Evidence for a strain-tuned topological phase transition in $ZrTe_5$, Sci. Adv. **5**, eaav9771 (2019).

[50] S. A. Miller, I. Witting, U. Aydemir, L. Peng, A. J. E. Rettie, P. Gorai, D. Y. Chung, M. G. Kanatzidis, M. Grayson, V. Stevanović, E. S. Toberer, and G. J. Snyder, Polycrystalline $ZrTe_5$ parametrized as a narrow-band-gap semiconductor for thermoelectric performance, Phys. Rev. Applied **9**, 014025 (2018).

[51] A. C. Niemann, J. Gooth, Y. Sun, F. Thiel, A. Thomas, C. Shekhar, V. Suß, C. Felser, and K. Nielsch, Magneto-thermoelectric characterization of a $HfTe_5$ micro-ribbon, Appl. Phys. Lett. **115**, 072109 (2019).

[52] H. Chi, C. Zhang, G. Gu, D. E. Kharzeev, X. Dai, and Q. Li, Lifshitz transition mediated electronic transport anomaly in bulk $ZrTe_5$, New J. Phys. **19**, 015005 (2017).

[53] M. Cutler and N. F. Mott, Observation of Anderson localization in an electron gas, Phys. Rev. **181**, 1336 (1969).

[54] G. S. Nolas, J. Sharp, and H. J. Godsmid, *Thermoelectrics: Basic Principles and New Materials Developments*, Springer Series in Material Science Vol. 45 (Springer, Heidelberg, 2001).

[55] Y.-Y. Lv, X. Li, L. Cao, D. Lin, S.-H. Yao, S.-S. Chen, S.-T. Dong, J. Zhou, Y. B. Chen, and Y.-F. Chen, Tunable resistance or magnetoresistance cusp and extremely large magnetoresistance in defect-engineered $HfTe_{5-\delta}$ single crystals, Phys. Rev. Applied **9**, 054049 (2018).

[56] A. B. Pippard, *Magnetoresistance in Metals* (Cambridge University Press, New York, 1989).